Available online at www.sciencedirect.com
ScienceDirect
Acta Materialia 56 (2008) 471–478
Acta MATERIALIA
www.elsevier.com/locate/actamat

On the formability of bulk metallic glass in its supercooled liquid state

Jan Schroers *

Department of Mechanical Engineering, Yale University, New Haven, CT 06511, USA

Received 28 February 2007; received in revised form 3 October 2007; accepted 4 October 2007
Available online 3 December 2007

Abstract

A method is introduced as a standard to characterize the formability, the maximum strain a bulk metallic glass (BMG) can undergo in its supercooled liquid state before it eventually crystallizes. When considering accuracy and practicality it was found that the maximum diameter to which a 0.1 cm^3 BMG sample can be formed during heating through the supercooled liquid temperature region under a constant load of 4500 N is best suited as a measure of formability. Among the ten different alloys considered, by far the highest formability was found for $Pt_{57.5}Cu_{14.7}Ni_{5.3}P_{22.5}$. More generally, the results suggest that fragile liquid behavior, large Poisson ratio, and a low glass transition temperature are attributes indicating good formability. Various parameters, as well as an analytical expression for the formability, are tested against the experimentally determined formability to assess the degree of correlation.

Keywords: Bulk metallic glass; Processing; Thermoplastic forming; Formability

1. Introduction

The existence of a supercooled liquid region (SCLR) is one of the most unique properties of BMGs and is a consequence of their strong resistance to crystallization. Upon heating into the SCLR the amorphous BMG first relaxes into a metastable liquid before it eventually crystallizes. It was already recognized during the early days of metallic glass research that a BMG can be formed in its SCLR [1,2]. This unique processing opportunity has been widely utilized for the purposes of surface replication [3–5], forming [6,7], micro-replication [5,8–14], extrusion [15–17], synthesis of amorphous foam [18], composite synthesis [19], and blow-molding [20–22].

The formability of a BMG in its supercooled liquid region is controlled by the temperature-dependent viscosity and the temperature-dependent crystallization time. The latter is a consequence of the metastable nature of BMGs in their SCLR which cause it to eventually crystallize. The time to reach crystallization, summarized in time–temperature–transformation diagrams, strongly depends on temperature and can range from seconds to hours [23–25]. During processing in the SCLR, crystallization has to be avoided since it prohibits flow and negates the attractive properties of the BMG-forming alloy in its amorphous state. The other parameter controlling the formability is the viscosity, which has been characterized for various BMG-forming alloys [26–29]. The temperature dependence of the viscosity among BMGs varies significantly. This reflects in the steepness index, $m = \frac{\mathrm{d}\log\eta}{\mathrm{d}T}\big|_{T=T_g}$, where values from $m = 69.6$ in $Ni_{60}Nb_{35}Sn_5$ [30] to $m = 38.3$ in $Zr_{41}Ti_{14}Cu_{12}Ni_{10}Be_{23}$ [31] have been reported. A large steepness index corresponds to fragile liquid behavior, while a small index corresponds to strong, nearly Arrhenius behavior.

Under isothermal conditions the formability of a BMG increases with increasing processing temperature [5]. It has been found that the highest isothermal formability can be achieved at the highest possible processing temperature, as long as crystallization can still be avoided [5]. An isothermal method to characterize the formability of a BMG in its SCLR would have significant drawbacks. The strong temperature dependence of the formability, together with the difficulty of absolute temperature measurement and control (which at least partially explains

* Tel.: +1 203 432 4346; fax: +1 203 432 6775.
E-mail address: jan.schroers@yale.edu

1359-6454/$30.00
doi:10.1016/j.actamat.2007.10.008

the large variation of published data on temperature-dependent viscosity and crystallization time), would make such a method inaccurate. Furthermore, the formability characterization at a specific and arbitrary isothermal temperature would not represent the overall formability since ΔT, m, and the temperature-dependent crystallization time have to be considered. These issues can be avoided when considering a standard which includes a constant heating condition rather than isothermal temperature.

Despite the key role of the formability for TPF, to date, no method has been developed to characterize BMG formability. Often the width of the SCLR, $\Delta T = T_x - T_g$ (T_g: glass transition temperature, T_x: crystallization temperature) is used as a parameter describing the formability of a BMG in its SCLR [7,32]. It has been suggested, however, that a normalized parameter, $S = \Delta T/T_l - T_g$, should better reflect the formability of a BMG, particularly when comparing different BMG alloy families [5]. Recently, Kato et al. introduced a parameter that also takes the temperature-dependent viscosity into account [33].

In this study, a method is introduced as a standard to characterize the formability of a BMG using the maximum diameter the BMG can be deformed to for a standardized set of processing parameters. This experimentally determined formability is compared with an analytical expression for the formability and discussed with reference to the above-mentioned parameters.

2. Experimental

The characterization was carried out on ten BMG-forming alloys: $Zr_{65}Al_{10}Ni_{10}Cu_{15}$ [34], $Pd_{43}Ni_{10}Cu_{27}P_{20}$ [35,36], $Zr_{58.5}Nb_{2.8}Ni_{12.8}Cu_{15.6}Al_{10.3}$ [37], $Zr_{41}Ti_{14}Cu_{12}Ni_{10}Be_{23}$ [38], $Zr_{44}Ti_{11}Cu_{10}Ni_{10}Be_{25}$ [28], $Au_{49}Ag_{5.5}Pd_{2.3}Cu_{26.9}Si_{16.3}$ [39], $Pt_{57.5}Cu_{14.7}Ni_{5.3}P_{22.5}$ [40], $Fe_{48}Cr_{15}Mo_{14}Er_2C_{15}B_6$ [41], $Mg_{65}Cu_{25}Y_{10}$ [42], and $Zr_{57}Nb_5Cu_{15.4}Ni_{12.6}Al_{10}$ [43]. These alloys cover a wide range of properties represented by fragility, glass transition temperature, Poisson ratio, ΔT, and T_l. A detailed alloy preparation is described in the corresponding references. The amorphous structure of each alloy in its as-cast condition was confirmed prior to the formability characterization by X-ray diffractometry (XRD) and thermal analysis using differential scanning calorimetry. Elastic constants were determined through ultrasonic measurements.

3. Method

The formability characterization method is sketched in Fig. 1. The BMG is positioned between platens which are forced against each other with a constant load. The characterization method is carried out under a constant heating rate between T_g and T_x. The formability of the alloy is characterized by the final diameter, d, to which the BMG deforms under the following conditions: a sample volume of 0.1 cm^3, a constant load of 4500 N, and a constant heating rate of 20 K min^{-1} applied in the temperature range between T_g and T_x. This set of parameters was found to result in the highest accuracy in determining the formability of a BMG. For example, Fig. 2 shows the dependence of the sample size on the final diameter. The BMGs' volume was chosen to provide the best compromise between minimizing size and minimizing the influence of the sample's volume on the maximum diameter. For all ten alloys considered in this article, the actual sample volume deviated less than 7% from the ideal volume, resulting in an effect on d, according to Fig. 2, of less than 3%. The initial shape of the BMG sample was found to have a negligible effect on d as long as the volume remained constant. This was confirmed by using different initial shapes with identi-

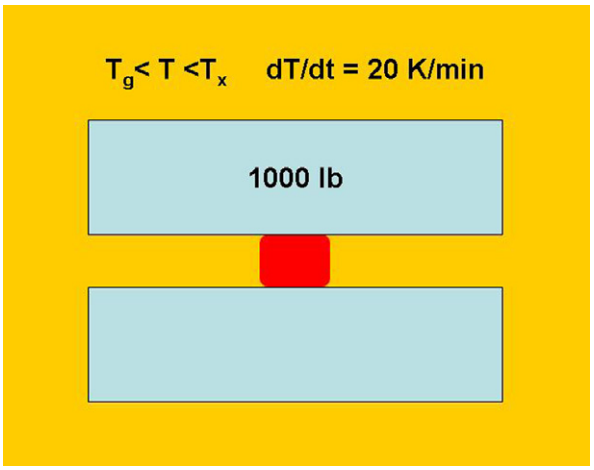

Fig. 1. Sketch of the formability characterization method. BMG of 0.1 cm^3 in volume is heated with 20 K min^{-1} through a temperature region between T_g and T_x under a compressive load of 4500 N. The maximum diameter to which the BMG is deformed during this process is taken as a measure for the formability.

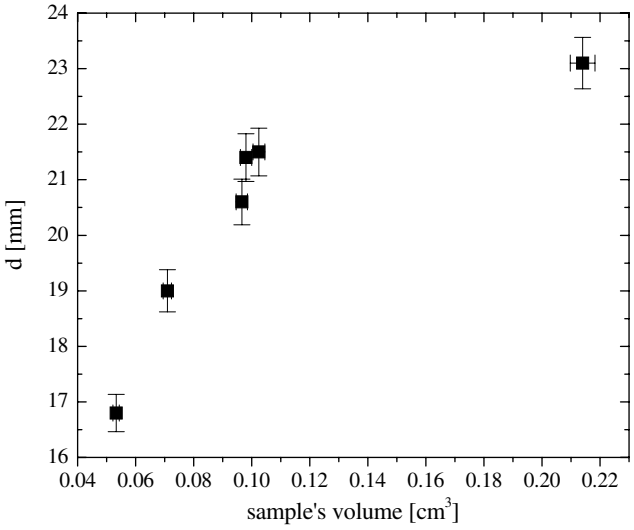

Fig. 2. Effect of the sample size on the maximum diameter to which the BMG deforms during characterization. $Zr_{44}Ti_{11}Cu_{10}Ni_{10}Be_{25}$ was used to determine for these data. A volume of 0.1 cm^3 was chosen as the best compromise between minimizing the sample size and minimizing the sensitivity to sample volume.

cal volume. A cube, a cylinder with an aspect ratio of 3, and a cylinder with an aspect ratio of 0.08 were formed to undistinguishable maximum diameter values. The surface finish of the platens was also observed to have a negligible effect on d as long as the roughness is small compared to the final thickness of the BMG. This was tested by comparing platens polished to a mirror finish with platens roughened by 320 grit sandpaper. However, adding lubricant changes the BMG contact conditions from stick to stick slip, thus influencing the final diameter.

It is well known that viscosity and crystallization time have a strong temperature dependence. Using a modeling approach it was also shown that the isothermal formability of a BMG-forming alloy depends strongly on temperature [5]. The maximum filling depth predicted by this model doubles approximately with every 20 K temperature increase [5]. In order to avoid such high-temperature sensitivity, the characterization method introduced in this work was not carried out isothermally but under a constant, 20 K min^{-1}, heating rate throughout the SCLR. As a consequence the maximum diameter was found to be significantly less sensitive to heating rate than it is to the isothermal processing temperature. This conclusion stems from the observation that variation of the heating rate between 10 K min^{-1} and 30 K min^{-1} did not noticeably influence the final diameter.

4. Results and discussion

The results of the characterization method are summarized in Fig. 3. A large variation of d values is observed among the BMGs considered here. The magnitude of d, together with other parameters, is summarized for the various alloys in Table 1. The largest d value, 32.7 mm, was observed for $Pt_{57.5}Cu_{14.7}Ni_{5.3}P_{22.5}$, and the smallest, $d = 6.2$ mm, was observed for $Fe_{48}Cr_{15}Mo_{14}Er_2C_{15}B_6$. Even the difference in formability of similar alloys such as $Zr_{58.5}Nb_{2.8}Ni_{12.8}Cu_{15.6}Al_{10.3}$ ($d = 14.65$ mm) and $Zr_{57}Nb_5Cu_{15.4}Ni_{12.6}Al_{10}$ ($d = 11.2$ mm) can be clearly resolved. As a side-effect this method also reveals information on the resistance to oxidation when processed in air in the temperature region between T_g and T_x. This is indicated and listed in Table 1 as the surface appearance of the BMG after completion of the formability characterization. From this appearance BMG alloys with high-resistance to oxidation can be identified which include

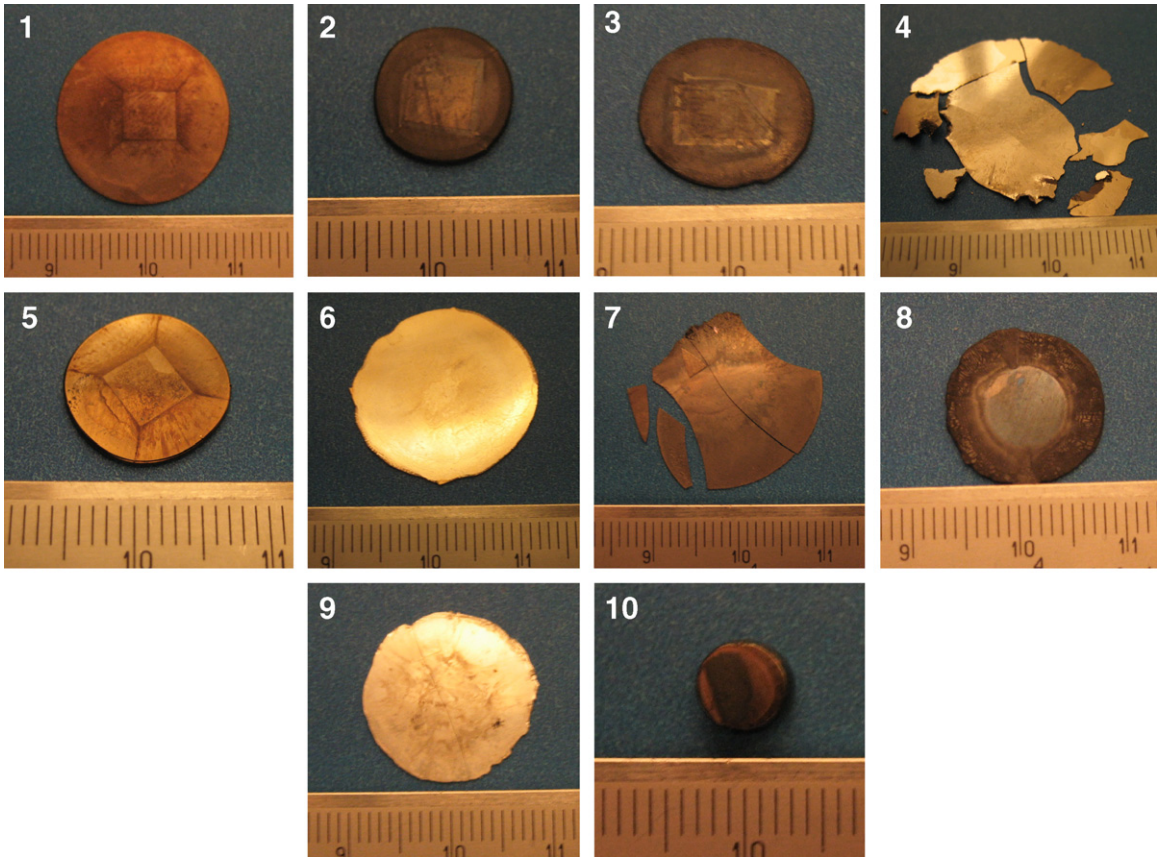

Fig. 3. Top view of the various BMGs after the formability characterization evaluation. All samples are deformed until they crystallize. Significant variations in the final diameter of the various BMGs can be observed. Surface appearance of the BMG alloys differs significantly from each other when processed in air, reflecting each BMG's resistance to oxidation. (1) $Zr_{44}Ti_{11}Cu_{10}Ni_{10}Be_{25}$; (2) $Zr_{57}Nb_5Cu_{15.4}Ni_{12.6}Al_{10}$, (3) $Zr_{58.5}Nb_{2.8}Ni_{12.8}Cu_{15.6}Al_{10.3}$; (4) $Pt_{57.5}Cu_{14.7}Ni_{5.3}P_{22.5}$; (5) $Zr_{41}Ti_{14}Cu_{12}Ni_{10}Be_{23}$; (6) $Au_{49}Ag_{5.5}Pd_{2.3}Cu_{26.9}Si_{16.3}$; (7) $Pd_{43}Ni_{10}Cu_{27}P_{20}$; (8) $Zr_{65}Al_{10}Ni_{10}Cu_{15}$; (9) $Mg_{65}Cu_{25}Y_{10}$; (10) $Fe_{48}Cr_{15}Mo_{14}Er_2C_{15}B_6$.

Table 1
Summary of the experimental results for the considered alloys

Alloy	T_g (°C)	T_x (°C)	ΔT (°C)	T_l (°C)	m	D^*	T_0 (°C)	υ	Appearance	d
$Zr_{41.2}Ti_{13.8}Cu_{12.5}Ni_{10}Be_{22.5}$	349	426	77	714	47.9	23.8[a]	117	0.352	Oxidized	14.1
$Zr_{44}Ti_{11}Cu_{10}Ni_{10}Be_{25}$	350	471	121	720	47.2	18.9[b]	117	0.349	Oxidized	20.5
$Zr_{57}Nb_5Cu_{15.4}Ni_{12.6}Al_{10}$	405	470	65	847	45.9	19.7[c]	164	0.379	Severely oxidized	11.2
$Zr_{58.5}Nb_{2.8}Cu_{15.6}Ni_{12.8}Al_{10.3}$	400	480	80	845	45.9	19.7C	164	0.377	Severely oxidized	14.65
$Pd_{43}Ni_{10}Cu_{27}P_{20}$	305	406	101	554	65.2[d]	12	92	0.396	Oxidized	25.55
$Au_{49}Ag_{5.5}Pd_{2.3}Cu_{26.9}Si_{16.3}$	130	184	54	382	52.8	16[e]	−23	0.406	Metallic shiny	21.56
$Pt_{57.5}Cu_{14.7}Ni_{5.3}P_{22.5}$	236	325	89	540	51.9	16.4[f]	63	0.43	Metallic shiny	32.7
$Fe_{48}Cr_{15}Mo_{14}Er_2C_{15}B_6$	573	620	47	1190				0.32	Severely oxidized	6.2
$Mg_{65}Cu_{25}Y_{10}$	155	219	64	484	42.7	22.1[g]	−13	0.305	Metallic	17.9
$Zr_{65}Al_{10}Ni_{10}Cu_{15}$	368	473	105	888	59.4	16.6[h]	164	0.377	Severely oxidized	13.6

Also shown are quantities used for the discussion of formability with various parameters. T_g, T_x, ΔT, T_l, and υ were determined using the same material used for the forming characterization. The steepness index was calculated from D^* by $m = 16 + 590/D^*$ [57]. The appearance describes the oxidation tendency of the various alloys during processing in air.

[a] [31].
[b] [28].
[c] [49].
[d] [29].
[e] [58].
[f] [51].
[g] [52].
[h] [53].

$Pt_{57.5}Cu_{14.7}Ni_{5.3}P_{22.5}$, $Au_{49}Ag_{5.5}Pd_{2.3}Cu_{26.9}Si_{16.3}$, and $Mg_{65}Cu_{25}Y_{10}$. Alloys with a large tendency to oxidize include $Fe_{48}Cr_{15}Mo_{14}Er_2C_{15}B_6$, $Zr_{65}Al_{10}Ni_{10}Cu_{15}$, and $Zr_{57}Nb_5Cu_{15.4}Ni_{12.6}Al_{10}$.

Theoretically, the formability of a BMG in its SCLR can be described by the maximum strain the BMG can undergo before it eventually crystallizes. Under the assumption of Newtonian behavior, i.e.

$$\sigma = \eta \cdot 3\dot{\varepsilon} \tag{1}$$

where σ is the flow stress and $\dot{\varepsilon}$ is the strain rate and under isothermal conditions the maximum strain can be calculated by integrating Eq. (1) between 0 and t_{cryst}

$$\int_0^{t_{cryst}} \dot{\varepsilon} dt = \int_0^{t_{cryst}} \frac{\sigma}{3\eta} dt \tag{2}$$

Thus the maximum strain achievable under isothermal conditions is given by

$$\varepsilon_{max} = t_{crsyt} \cdot \frac{\sigma}{3\eta} \tag{3}$$

Here, the quantity reflecting the isothermal formability, F_{iso} is given by

$$F_{iso} = \frac{t_{cryst}}{3\eta} \tag{4}$$

Eq. (4) reveals the strong temperature dependence of the formability. The viscosity of a BMG changes roughly by an order of magnitude every 20 K [28], while the crystallization time changes by an order of magnitude every 50 K [28]. For example, an error of 10 K in the temperature measurement would result, according to Eq. (5), in an error of 40% in F. This emphasizes the need for a less temperature-sensitive method such as the constant heating technique introduced in this work. The formability parameter can be extended to constant heating conditions, F, by modifying Eqs. (3) and (4)

$$F = \frac{1}{3\dot{T}} \int_{T_g}^{T_x(\dot{T})} \frac{1}{\eta(T)} dT, \tag{5}$$

where T_x is the heating-rate-dependent crystallization temperature. For the temperature-dependent viscosity, the Vogel–Fulcher–Tamann (VFT) expression is used

$$\eta = \eta_0 \cdot \exp\left(\frac{D^* T_0}{T - T_0}\right) \tag{6}$$

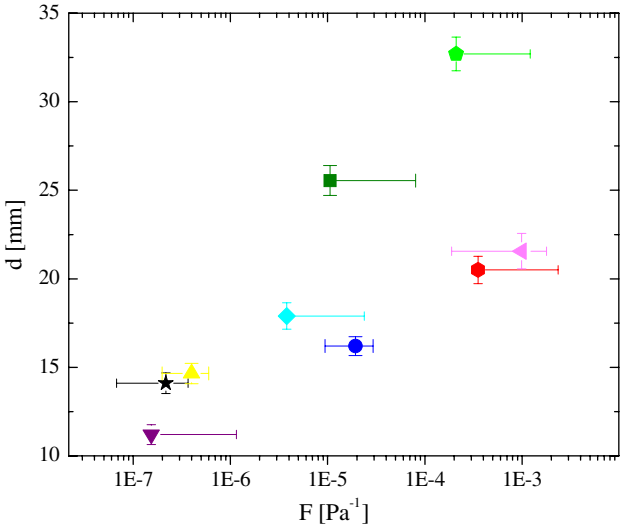

Fig. 4. Experimentally determined formability, d plotted vs F (see Eq. (5)). ■: $Pd_{43}Ni_{10}Cu_{27}P_{20}$; ♦: $Mg_{65}Cu_{25}Y_{10}$; ◀: $Au_{49}Ag_{5.5}Pd_{2.3}Cu_{26.9}Si_{16..3}$; ▼: $Zr_{57}Nb_5Cu_{15.4}Ni_{12.6}Al_{10}$; ▲: $Zr_{58.5}Nb_{2.8}Ni_{12.8}Cu_{15.6}Al_{10.3}$; ●: $Zr_{65}Al_{10}Ni_{10}Cu_{15}$; ★: $Zr_{41}Ti_{14}Cu_{12}Ni_{10}Be_{23}$; ⬢: $Zr_{44}Ti_{11}Cu_{10}Ni_{10}Be_{25}$; ⬟: $Pt_{57.5}Cu_{14.7}Ni_{5.3}P_{22.5}$.

Here D^* denotes the fragility parameter and T_0 the VFT temperature where the barrier to flow goes to infinity. The pre-exponential factor, $\eta_0 = \frac{h}{v_m}$ (h is Planck's constant, v_m is atomic volume), can be well approximated by 4×10^{-5} Pa s [44]. By substituting Eq. (6) into Eq. (5) and using the parameters shown in Table 1, F has been calculated and plotted in Fig. 4 against the experimentally determined formability d.

Calculating the formability of a BMG as shown above requires measurement of the temperature-dependent viscosity as well as thermal analysis to determine the crystallization behavior. In order to identify a parameter of more practical relevance we will now discuss the correlation of the experimentally determined formability with various parameters, of which several were used in the past to describe formability of BMGs. Fig. 5 depicts the experimentally determined formability plotted against T_g/T_l, ΔT, $\Delta T/T_g$, $m\Delta T/T_g$ and $\Delta T/(T_l - T_g)$. To compare the correlation of these parameters with d, a linear fit was performed and the standard deviation, SD, was used as a measure of the correlation. The smallest SD, and hence the strongest correlation, was found between d and S (SD = 4.73), followed by SD = 4.99 between d and F, SD = 5.13 between $m\Delta T/T_g$ and d, and SD = 5.4 between $\Delta T/T_g$ and d. The weakest correlations were found between d and T_g/T_l (SD = 7.05) and between d and ΔT (SD = 6.97). Also indicated in Figs 4 and 5 is the magnitude of the errors. For d, the error was given by the variation of the maximum diameter from at least three identical experiments, and also from the deviation from a circular (final) shape and from the 0.1 cm^3 target volume (see Fig. 2). The error for the parameters $\Delta T/T_g$, T_g/T_l, $m\Delta T/T_g$, S, and F was calculated using error propagation with individual errors for T_g, T_x, T_l, D^*, and T_o. From a tangential determination of the values for T_g, T_x, and T_l, we determined the following individual errors: $\Delta T_g = 3$ K,

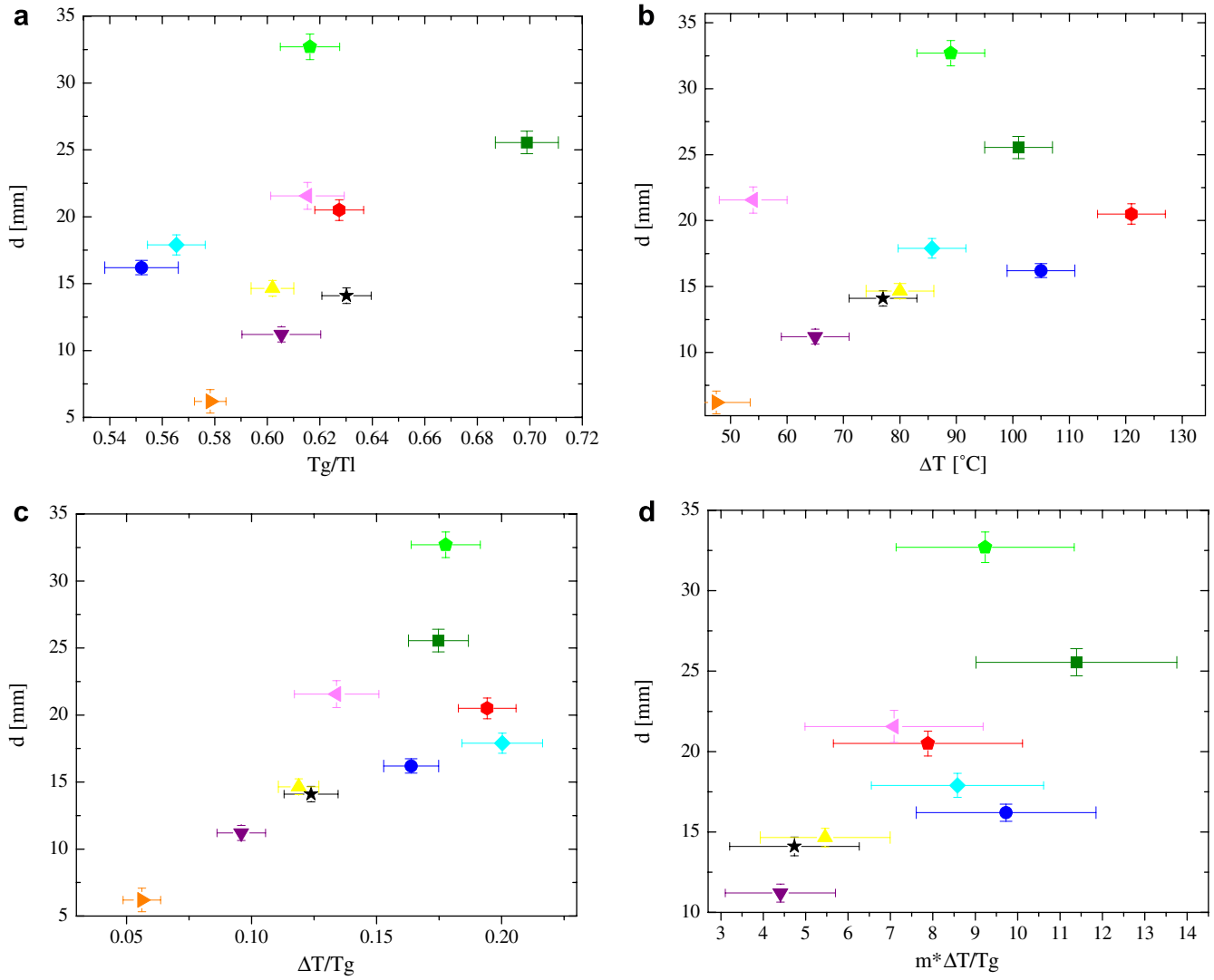

Fig. 5. Experimentally determined formability, d vs various parameters. (a) T_g/T_l, (b) ΔT, (c) $\Delta T/T_g$; (d) $m\Delta T/T_g$; (e) S, (f) T_g; (g) m; (h) υ. ■: $Pd_{43}Ni_{10}Cu_{27}P_{20}$; ◆: $Mg_{65}Cu_{25}Y_{10}$; ►: $Fe_{48}Cr_{15}Mo_{14}Er_2C_{15}B_6$; ◄: $Au_{49}Ag_{5.5}Pd_{2.3}Cu_{26.9}Si_{16.3}$; ▼: $Zr_{57}Nb_5Cu_{15.4}Ni_{12.6}Al_{10}$; ▲: $Zr_{58.5}Nb_{2.8}Ni_{12.8}Cu_{15.6}Al_{10.3}$; ●: $Zr_{65}Al_{10}Ni_{10}Cu_{15}$; ★: $Zr_{41}Ti_{14}Cu_{12}Ni_{10}Be_{23}$; ⬢: $Zr_{44}Ti_{11}Cu_{10}Ni_{10}Be_{25}$; ⬟: $Pt_{57.5}Cu_{14.7}Ni_{5.3}P_{22.5}$.

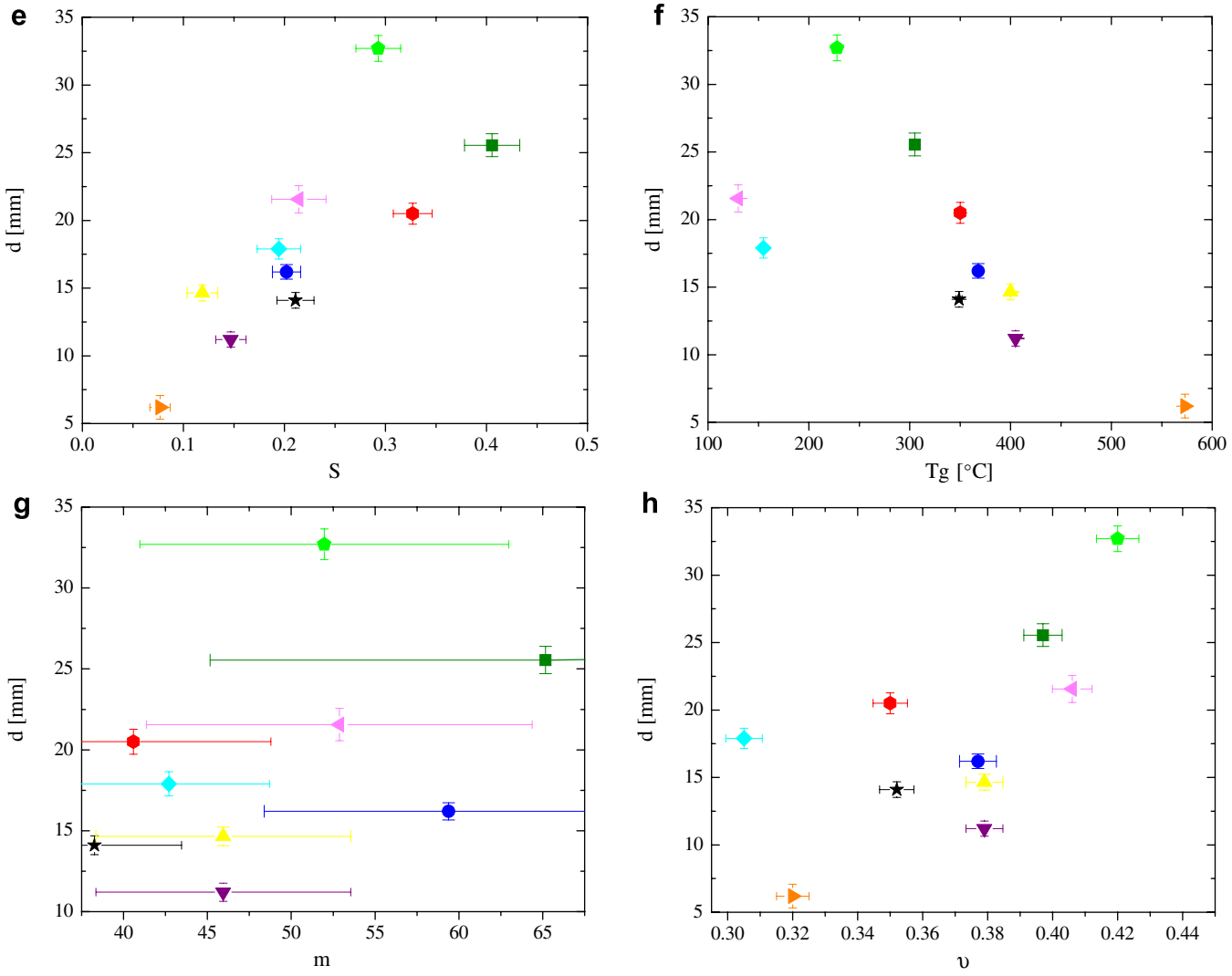

Fig. 5 (*continued*)

$\Delta T_x = 3$ K, and $\Delta T_l = 5$ K. For the Poisson ratio the error was determined from the scattering of data of at least three measurements to be $\Delta\upsilon = 1.5\%$. The error for m was estimated from published data on the steepness index for $Zr_{41}Ti_{14}Cu_{12}Ni_{10}Be_{23}$, which vary between $m = 47.9$ [28] and $m = 40.8$ [45]. This corresponds to an error for D^* of 5 and an error for T_0 of 50 K.

We will know discuss the correlation between d and the various parameters.

The reduced glass transition temperature introduced by Turnbull [46], T_g/T_l, has been used in the past to describe an alloy's glass-forming ability, and the correlation has been widely confirmed [47,48]. Since in general T_g/T_l does not even show a correlation with ΔT [39,48], the very weak correlation between T_g/T_l and d, as shown in Fig. 5a, is not surprising, and we can therefore conclude that the glass-forming ability of a BMG is not a good indicator of its formability.

The width of the supercooled liquid region, ΔT, has been widely used in the past to characterize the formability of a BMG in its SCLR (see e.g. Refs. [7,32]). An increase in ΔT allows a BMG to be processed at lower viscosities and increases the overall forming time available. The present results shown in Fig. 5b, however, reveal that ΔT has only a weak correlation with the formability in particular when comparing alloys with different T_g values. For example, $Pt_{57.5}Cu_{14.7}Ni_{5.3}P_{22.5}$ and $Au_{49}Ag_{5.5}Pd_{2.3}Cu_{26.9}Si_{16.3}$, with their low T_g values, both exhibit significantly better formability than is suggested by the ΔT of each. $Zr_{65}Al_{10}Ni_{10}Cu_{15}$ and $Zr_{44}Ti_{11}Cu_{10}Ni_{10}Be_{25}$, on the other hand, are less formable than is suggested by their ΔT values because they both exhibit a high T_g. The most dramatic comparison can be found between $Au_{49}Ag_{5.5}Pd_{2.3}Cu_{26.9}Si_{16.3}$ and $Zr_{44}Ti_{11}Cu_{10}Ni_{10}Be_{25}$; though the former exhibits a ΔT of 54 K, its formability actually exceeds that of $Zr_{44}Ti_{11}Cu_{10}Ni_{10}Be_{25}$, which has a ΔT of 121 K.

When normalizing ΔT to T_g, the correlation with d is significantly better (see Fig. 5c). This can be explained by considering viscosity in the framework of relative fragility using a so-called "Angell plot". This is a modified

Arrhenius plot in which the viscosities measured for different glass-forming systems are compared using an inverse temperature axis which is multiplied by the temperature at which the viscosity of each respective alloy is 10^{12} Pa s. Therefore, all curves meet at 10^{12} Pa s, and this value is thus defined to be the glass transition viscosity for each system. When plotted in such a way, ΔT has to be normalized to T_g. The temperature dependence of the viscosity is, however, not reflected in this parameter. This is evidenced by the fact that the formability is underrepresented by $\Delta T/T_g$ for the fragile BMGs such as $Pt_{57.5}Cu_{14.7}Ni_{5.3}P_{22.5}$, $Au_{49}Ag_{5.5}Pd_{2.3}Cu_{26.9}Si_{16.3}$, and $Pd_{43}Ni_{10}Cu_{27}P_{20}$, but is overrepresented by $\Delta T/T_g$ for the strong BMGs like $Mg_{65}Cu_{25}Y_{10}$ and $Zr_{44}Ti_{11}Cu_{10}Ni_{10}Be_{25}$.

The temperature dependence of the viscosity can be considered by multiplying $\Delta T/T_g$ with the steepness index [33]. Within the Angell plot, this parameter approximates the viscosity between T_g and T_x as linear. Even though a large scatter in the correlation is observed (Fig. 5d), no systematic deviation from the correlation can be found. It should be mentioned that the steepness index was not determined in this work but was taken from various sources [28,29,31,49–53]. The large error for m might be responsible for the large scatter in $m\Delta T/T_g$ when plotting against d.

A different approach is taken by the parameter $S = \Delta T/T_l - T_g$, which was found to have the best correlation with d of SD = 4.73 as shown in Fig. 5e. This parameter is justified by the observation that viscosity values are similar for BMGs at their liquidus temperature [31]. Therefore, the temperature dependence of the viscosity is accounted for by using $T_l - T_g$. This results in a tremendous practical advantage of S over $m\Delta T/T_g$ and also F. The determination of $m\Delta T/T_g$ and F requires both rheological and thermal analysis data, while S is solely determined using thermal analysis data. It is important to note, though, that deviations from Arrhenius behavior reflected in BMG fragility are not being considered in the S parameter.

Surprisingly, it was found that when plotting the formability against T_g, a clear trend can be observed with an SD of 5.8. This correlation, shown in Fig. 5f, is unexpected to the author. For example, no correlation between T_g and the steepness index or between T_g and ΔT was found for the considered alloys. A wider range of alloys must be studied to investigate this correlation further.

It was also noticed that fragility and Poisson ratio of the BMG correlate with the formability. The correlation between m and d (Fig. 5g) and υ and d (Fig. 5h) of 6.4 and 6.14, respectively, is even stronger than the correlation between ΔT and d of 6.97. A correlation between m and d seems obvious when looking solely on the effect of viscosity since a large m results in a low viscosity at same T/T_g. However, m can have an opposite effect on the crystallization kinetic. Even though some exceptions have been reported (see e.g. Ref. [28]) a large ΔT often reflects good glass-forming ability and vice versa (see e.g. Ref. [54]). Together with the observation that good glass-forming ability seems to be correlated with strong liquid behavior one can conclude that a fragile liquid should result in a small ΔT. The observed correlation suggests that the effect of fragility on the temperature-dependent viscosity dominates over the effect on the crystallization time. Recently, it was also observed that fragile glasses including metallic glasses tend to have a higher Poisson ratio [55,56]. This finding, together with the observed correlation between m and d, suggest, as experimentally observed, a correlation between υ and d. It should be mentioned, however, that the correlation between fragility and d should be stronger than between d and Poisson ratio since these two quantities are only indirectly correlated through the fragility.

5. Conclusions

A method was introduced as a standard to characterize the formability of a BMG in its supercooled liquid region. The accuracy and practicality of this method enable to study a wide range of BMGs where even the formability of similar alloys can be resolved. The results were also used to identify parameters that reflect the formability of BMGs in their supercooled liquid region. It was revealed that the width of the supercooled liquid region normalized by the width of the undercooled liquid region shows the best correlation with formability. This parameter is also desirable for practical reasons since it can be obtained using only thermal analysis.

Acknowledgements

Liquidmetal Technologies and Professor Wei-Hua Wang are gratefully acknowledged for providing some of the alloys. Fruitful discussions with Dr. Sven Bossuyt, Professor Corey O'Hern, and Dr. Theodore A. Waniuk are also gratefully acknowledged.

References

[1] Leamy HJ, Chen HS, Wang TT. Metall Trans 1972;3:699.
[2] Pampillo CA, Chen HS. Mater Sci Eng 1974;13:181–8.
[3] Nishiyama N, Inoue A. Mater Trans Jim 1999;40:64–71.
[4] Schroers J, Paton N. Adv Mater Process 2006;164:61–3.
[5] Schroers J. Jom 2005;57:35–9.
[6] Zhang B, Zhao DQ, Pan MX, Wang WH, Greer AL. Phys Rev Lett 2005;94.
[7] Ponnambalam V, Poon SJ, Shiflet GJ. J Mater Res 2004;19:3046–52.
[8] Saotome Y, Miwa S, Zhang T, Inoue A. J Mater Process Technol 2001;113:64–9.
[9] Saotome Y, Itoh K, Zhang T, Inoue A. Scripta Mater 2001;44:1541–5.
[10] Jeong HW, Hata S, Shimokohbe A. J Microelectromech Sys 2003;12:42–52.
[11] Saotome Y, Noguchi Y, Zhang T, Inoue A. Mater Sci Eng A – Struct Mater Propert Microstruct Process 2004;375(77):389–93.
[12] Pryds NH. Mater Sci Eng A – Struct Mater Propert Microstruct Process 2004;375–77:186–93.
[13] Schroers J, Pham Q, Desai A. J Microelectromech Sys 2007;16:240–7.
[14] Schroers J, Nguyen T, O'Keeffe S, Desai A. Mater Sci Eng A – Struct Mater Propert Microstruct Process 2007;449:898–902.

[15] Kawamura Y, Kato H, Inoue A, Masumoto T. Appl Phys Lett 1995;67:2008–10.
[16] Sordelet DJ, Rozhkova E, Huang P, Wheelock PB, Besser MF, Kramer MJ, et al. J Mater Res 2002;17:186–98.
[17] Karaman I, Robertson J, Im JT, Mathaudhu SN, Luo ZP, Hartwig KT. Metall Mater Trans A – Phys Metall Mater Sci 2004;35A: 247–56.
[18] Schroers J, Veazey C, Demetriou MD, Johnson WL. J Appl Phys 2004;96:7723–30.
[19] Schroers J, Nguyen T, Croopnick GA. Scripta Mater 2007;56:177–80.
[20] Kim WJ, Sa Y, Lee JB, Jeong HG. Intermetallics 2006;14:1391–6.
[21] Soejima H, Nishiyama N, Takehisa H, Shimanuki M, Inoue A. J Metastable Nanocrystal Mater 2005;24:531.
[22] Schroers J, Pham Q, Peker A, Paton N, Curtis RV. Scripta Mater 2007;57:341–4.
[23] Schroers J, Wu Y, Busch R, Johnson WL. Acta Mater 2001;49:2773–81.
[24] Schroers J, Wu Y, Johnson WL. Philos Mag A – Phys Condens Mat Struct Defect Mechan Propert 2002;82:1207–17.
[25] Schroers J, Busch R, Bossuyt S, Johnson WL. Mater Sci Eng A – Struct Mater Propert Microstruct Process 2001;304:287–91.
[26] Busch R, Bakke E, Johnson WL. Acta Mater 1998;46:4725–32.
[27] Waniuk TA, Busch R, Masuhr A, Johnson WL. Acta Mater 1998;46:5229–36.
[28] Waniuk T, Schroers J, Johnson WL. Phys Rev B 2003;67:184203.
[29] Fan GJ, Fecht HJ, Lavernia EJ. Appl Phys Lett 2004;84:487–9.
[30] Shadowspeaker L, Busch R. Appl Phys Lett 2004;85:2508–10.
[31] Mukherjee S, Schroers J, Zhou Z, Johnson WL, Rhim WK. Acta Mater 2004;52:3689–95.
[32] Zhang W, Inoue A. Mater Trans 2003;44:2220–3.
[33] Kato H, Wada T, Hasegawa M, Saida J, Inoue A, Chen HS. Scripta Mater 2006;54:2023–7.
[34] Inoue A, Zhang T, Masumoto T. Mater Trans Jim 1990;31:177–83.
[35] Nishiyama N, Inoue A. Acta Mater 1999;47:1487–95.
[36] Lu IR, Wilde G, Gorler GP, Willnecker R. J Non-Crystal Solids 1999;252:577–81.
[37] Hays CC, Schroers J, Johnson WL, Rathz TJ, Hyers RW, Rogers JR, et al. Appl Phys Lett 2001;79:1605–7.
[38] Peker A, Johnson WL. Appl Phys Lett 1993;63:2342–4.
[39] Schroers J, Lohwongwatana B, Johnson WL, Peker A. Appl Phys Lett 2005;87:61912.
[40] Schroers J, Johnson WL. Appl Phys Lett 2004;84:3666–8.
[41] Ponnambalam V, Poon SJ, Shiflet GJ. J Mater Res 2004;19:1320–3.
[42] Inoue A, Kato A, Zhang T, Kim SG, Masumoto T. Mater Trans Jim 1991;32:609–16.
[43] Lin XH, Johnson WL. J Appl Phys 1995;78:6514–9.
[44] Glasstone S. The theory of rate processes. New York: McGraw-Hill; 1941.
[45] Mukherjee S, Schroers J, Johnson WL, Rhim WK. Phys Rev Lett 2005;94:245501.
[46] Turnbull D. Contemp Phys 1969;10:473.
[47] Lu ZP, Tan H, Li Y, Ng SC. Scripta Mater 2000;42:667–73.
[48] Waniuk TA, Schroers J, Johnson WL. Appl Phys Lett 2001;78:1213–5.
[49] Gallino I, Shah MB, Busch R. Acta Mater 2007;55:1367–76.
[50] Lohwongwatana B. unpublished results, 2007.
[51] Legg BA, Schroers J, Busch R. Acta Mater 2007;55:1109.
[52] Busch R, Liu W, Johnson WL. J Appl Phys 1998;83:4134–41.
[53] Busch R, Masuhr A, Bakke E, Johnson WL. Mechan Alloy, Metastable Nanocrystal Mater, Part 2 1998;269(2):547–52.
[54] Inoue A, Zhang T, Masumoto T. J Non-Crystal Solids 1993;156:473–80.
[55] Novikov VN, Sokolov AP. Nature 2004;431:961–3.
[56] Wang WH. J Appl Phys 2006;99.
[57] Bohmer R, Ngai KL, Angell CA, Plazek DJ. J Chem Phys 1993;99:4201–9.
[58] Schroers J, Lohwongwatana B, Johnson WL, Peker A. Mater Sci Eng A – Struct Mater Propert Microstruct Process 2007;449:235–8.